Physics of Plasmas

RESEARCH ARTICLE | AUGUST 12 2026

A first-principles theoretical model of the reconnection rate in non-steady magnetic reconnection

Quanming Lu ; Yukang Shu ; San Lu ; Shiyong Huang; Shihang Hu ; Rongsheng Wang

Phys. Plasmas 33, 082109 (2026)
https://doi.org/10.1063/5.0338261

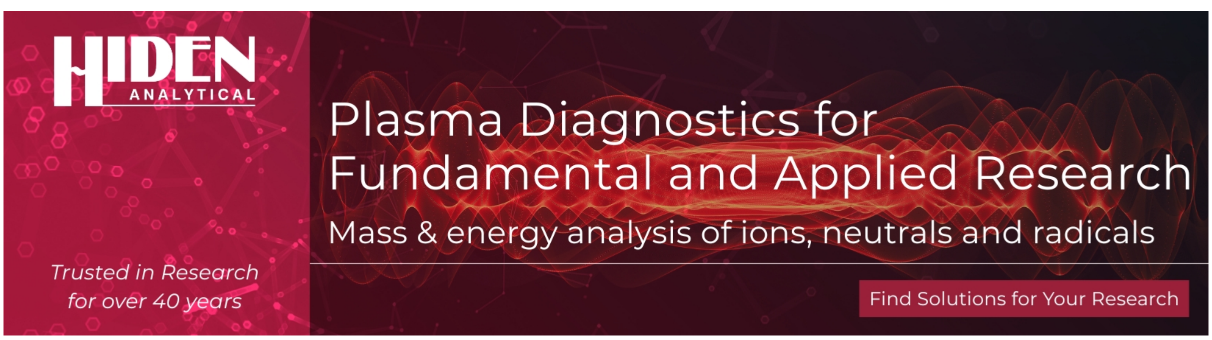

Physics of Plasmas ARTICLE pubs.aip.org/aip/pop

A first-principles theoretical model of the reconnection rate in non-steady magnetic reconnection

Cite as: Phys. Plasmas **33**, 082109 (2026); doi: 10.1063/5.0338261
Submitted: 11 April 2026 · Accepted: 26 July 2026 ·
Published Online: 12 August 2026

View Online Export Citation CrossMark

Quanming Lu,[1,2,a)] Yukang Shu,[1,2] San Lu,[1,2] Shiyong Huang,[3] Shihang Hu,[1,2] and Rongsheng Wang[1,2]

AFFILIATIONS

[1]Deep Space Exploration Laboratory/School of Earth and Space Sciences, University of Science and Technology of China, Hefei 230026, China

[2]Collaborative Innovation Center of Astronautical Science and Technology, Harbin, China

[3]School of Earth and Space and Technology, Wuhan University, Wuhan, China

[a)]Author to whom correspondence should be addressed: qmlu@ustc.edu.cn

ABSTRACT

As a key parameter in magnetic reconnection, the reconnection rate determines the speed at which magnetic energy is converted into plasma kinetic energy. It is well established that the reconnection rate of collisionless magnetic reconnection is on the order of 0.1—a value sufficiently high to account for various explosive phenomena in space environments, such as solar flares and geomagnetic substorms. Recently, Lu *et al.* [Sci. Bull. **70**, 2766 (2025)] proposed a first-principles theoretical model of the reconnection rate during non-steady collisionless reconnection in a Harris-type current sheet. As magnetic reconnection proceeds, the ion and electron outflows increase continuously over time. Plasma becomes depleted in the electron and ion diffusion regions, while the magnetic field piles up downstream, causing the opening angles of the diffusion regions to grow continuously. As a result, the reconnection rate rises progressively and eventually reaches a peak value, which is approximated as $0.2\sqrt{n_0/n_b}$ (where n_0 is the peak density in the current sheet and n_b is the density of the background plasma) and exhibits no dependence on the ion-to-electron mass ratio. However, in that model, the ion and electron outflows are solely governed by the Lorentz force term. In the present paper, we additionally incorporate contributions from the electric field and pressure gradient terms and analyze their combined influence on the electron and ion outflows and then the peak reconnection rate. Our results indicate that the electric field and pressure gradient terms weaken electron and ion outflows, which, in turn, reduces the peak reconnection rate. In the new model, the peak reconnection rate is roughly $1/\sqrt{5}$ times that in Lu *et al.* [Sci. Bull. **70**, 2766 (2025)], which scales approximately as $0.09\sqrt{n_0/n_b}$.

I. INTRODUCTION

This reconnection rate—defined as the quantity of magnetic flux produced per unit time (or equivalently, the reconnection electric field in the out-of-plane direction) at the reconnection site—stands as one of the key characteristics of magnetic reconnection, which is a fundamental plasma process for energy conversion from magnetic energy to plasma kinetic and thermal energy via the rearrangement of magnetic field topology.[1,2] Magnetic reconnection has long been recognized as the mechanism driving explosive phenomena in space, astrophysical, and laboratory plasmas, and its energy conversion efficiency is quantitatively determined by the reconnection rate.[3–11] Consequently, substantial efforts have been dedicated to developing theoretical models for the quantitative prediction of this rate.[12–19]

The Sweet-Parker model is the first theoretical model for steady magnetic reconnection.[12,13] Based on magnetohydrodynamics (MHD), where ions and electrons are coupled together, it assumes steady magnetic flux reconnection and an incompressible plasma. Magnetic energy dissipation occurs in the diffusion region via Ohmic heating, with the predicted reconnection rate proportional to $S^{-1/2}$ (where S denotes the Lundquist number). Notably, the Lundquist number is typically extremely large in space and astrophysical plasmas, resulting in a predicted reconnection rate that is too low to explain explosive phenomena.[20] A viable solution is to incorporate ion and electron kinetics, giving rise to what is termed collisionless magnetic reconnection. The diffusion region in this regime features a two-layer structure: an ion diffusion region (IDR) with an electron diffusion region (EDR) at its center.[21–27] In the EDR, both ions and electrons are unmagnetized,[6,22,28–32] whereas electrons become magnetized within the IDR.[33–39] Numerous simulations and observations have confirmed that, in collisionless magnetic reconnection, the normalized reconnection rate—based on a properly defined reconnecting magnetic field and Alfvén speed—is on the order of 0.1.[15,36,40–44] This value is sufficiently high to account for explosive phenomena in space and astrophysical plasmas, such as solar flares and magnetospheric substorms.[45]

Although the fast reconnection rate in collisionless magnetic reconnection has attracted significant attention, its underlying mechanism remains a matter of ongoing debate.[16,17] Liu *et al.*[18] proposed a theoretical model for the reconnection rate of collisionless magnetic reconnection under steady-state conditions, assuming an incompressible plasma. Energy conversion within the IDR induces the enhancement of thermal pressure at the reconnection site, and then the depletion of the magnetic field in order to maintain the force-balance condition. At last, a sufficiently large opening angle of the upstream magnetic field is developed, which enables the reconnection rate to be on the order of 0.1. The effect of thermal pressure is taken into account in the model developed by Li and Liu,[46] and the predicted reconnection rate drops as the plasma β becomes larger. Recently, in the analytical model proposed by Zhan *et al.*,[47] the electric field and thermal pressure are shown to be crucial in modulating the reconnection rate in electron-only reconnection.[48] In these models, magnetic reconnection is assumed to be in a steady state. However, magnetic reconnection always proceeds in a non-steady state, which has been demonstrated by both numerical simulations and satellite observations.[22,25,49,50] In non-steady magnetic reconnection, a pair of dipolarization fronts (DFs) due to the pileup of magnetic field is formed downstream of the IDR.[51–57] Lu *et al.*[19] realized that the plasma is depleted in the EDR during the reconnection evolution, while the magnetic field is piled up in the downstream of the IDR, which makes the opening angle of the EDR larger and larger. It leads to the enhancement of the reconnection rate until a peak value on the order of 0.1 is reached.

However, the pressure gradient and electric field are neglected in the model developed by Lu *et al.*.[19] In this paper, by including these effects in the force-balance equation of ion and electron outflows, we obtain the ion and electron outflow velocities as a function of the opening angles of the IDR and EDR and, at last, provide the prediction of the reconnection rate.

The remainder of this paper is organized as follows. In Sec. II, we present the details of the model. In Sec. III, the simulation results are utilized to verify the validity of our model. The summary and discussion are given in Sec. IV.

II. THEORETICAL MODEL

The diffusion region of collisionless magnetic reconnection exhibits a two-layer structure, with the EDR embedded at the core of the IDR. The reconnection electric field at the X line is almost the same as that on the downstream boundary of the EDR, and we will use the latter one ($E_{yE} = V_{exE}B_{zE}$) to investigate the evolution of the reconnection rate [$R = E_{yE}/(V_A B_0)$]. The diagram of the electron and ion diffusion regions is plotted in Fig. 1. Here, the aspect ratios of the EDR and IDR are assumed to be the same, which is denoted by S_L.

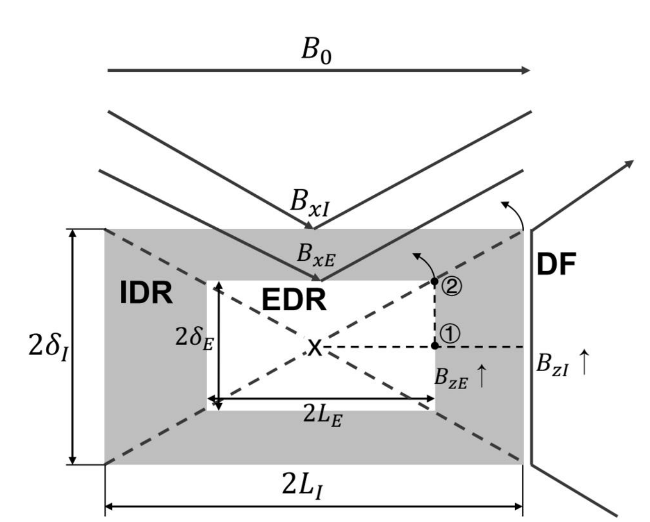

FIG. 1. Diagram of the EDR and IDR. B_0 is the asymptotic magnetic field of the current sheet, and B_{xI} and B_{xE} are the magnetic fields just upstream of the IDR and EDR.

The x component of the electron momentum equation along the line $z = 0$ can be described as follows:

$$n_e m_e\left(\frac{\partial V_{ex}}{\partial t} + V_{ex}\frac{\partial V_{ex}}{\partial x}\right) = j_{ey}B_z - en_eE_x - \frac{\partial P_{exx}}{\partial x}. \quad (1)$$

In general, the time derivative of the electron outflow velocity is negligible.[57–59] Then, Eq. (1) can be written as,

$$n_e m_e V_{ex}\frac{\partial V_{ex}}{\partial x} = j_{ey}B_z - en_eE_x - \frac{\partial P_{exx}}{\partial x}. \quad (2)$$

The right-hand side of the equation illustrates the contributions from the Lorentz force, electric field, and pressure gradient terms. According to $\nabla \times \boldsymbol{B} = \mu_0\boldsymbol{J}$, we can obtain $\frac{\partial B_x}{\partial z} - \frac{\partial B_z}{\partial x} = \mu_0(j_{ey} + j_{iy})$. During the evolution of magnetic reconnection, the electron current density is much larger than the ion current density ($j_{ey} \gg j_{iy}$) in the EDR when the reconnection rate approaches its peak value. We assume that the magnetic field linearly changes in the EDR, and the aspect ratio is $S_L = \frac{B_{zE}}{B_{xE}} = \frac{\delta_E}{L_E}$. Then, $j_{ey} \approx \frac{1}{\mu_0}\frac{B_{xE}}{\delta_E}(1 - \frac{\delta_E^2}{L_E^2})$, and the first term on the right-hand side of Eq. (2) is approximately expressed as $\frac{B_{xE}^2}{2\mu_0 L_E}\left(1 - \frac{\delta_E^2}{L_E^2}\right)$.

In the theoretical model developed by Lu *et al.*,[19] only the Lorentz force term is retained. In this paper, we further consider the contributions from the electric field and pressure gradient terms and analyze their combined influence on the electron outflow in the EDR. Based on Faraday's law, we can get $\oint \boldsymbol{E}\cdot d\boldsymbol{l} = \frac{\partial}{\partial t}\int\int \boldsymbol{B}\cdot d\boldsymbol{s}$ along the path X-1–2-X. When the reconnection rate approaches its peak value, $\frac{\partial}{\partial t}\int\int \boldsymbol{B}\cdot d\boldsymbol{s} \approx 0$. At the same time, the parallel electric field is much smaller than the perpendicular electric field,[60,61] and then, we can get $-\int_X^1 en_eE_x dx \approx \int_1^2 en_eE_z dz \approx -en_eV_{exE}\int_1^2 B_y dz$. According to $(\nabla\times\boldsymbol{B})_{\boldsymbol{x}} = \mu_0 j_x$, we obtain $\frac{\partial B_y}{\partial z} = -\mu_0 j_x \approx \mu_0 en_eV_{ex}$ in the EDR and $B_y \approx \mu_0 en_eV_{ex}z$, which can be approximately considered to change linearly with z. At last, the second term on the right-hand side of Eq. (2) is about $-\frac{1}{2}\mu_0 e^2 n_e^2 V_{exE}^2 \delta_E^2/L_E$.

The reconnection electric field is approximately uniform in the EDR, and it is E_{yX}. The work done to the electrons in the EDR is $\int\int E_{yX} j_{ey} dxdz \approx \int\int V_{exE} \quad B_{zE}\frac{1}{\mu_0}\left(\frac{\partial B_x}{\partial z}-\frac{\partial B_z}{\partial x}\right)dxdz \approx \frac{1}{\mu_0}V_{exE}B_{zE}B_{xE} \times\left(1-\frac{\delta_E^2}{L_E^2}\right)L_E$. Although electrons within the EDR remain unmagnetized and feature pronounced pressure agyrotropy,[32,62] most of the dissipated energy is anticipated to be converted into outward electron enthalpy flux departing the EDR.[57] Under the assumption of identical diagonal components for the electron pressure tensor, this enthalpy flux reads $\frac{5}{2}p_{exxE}V_{exE}\delta_E$. Then, $p_{exxE} \approx \frac{2}{5\mu_0}B_{xE}B_{zE}\left(1-\frac{\delta_E^2}{L_E^2}\right)\frac{L_E}{\delta_E} = \frac{2B_{xE}^2}{5\mu_0}\left(1-\frac{\delta_E^2}{L_E^2}\right)$, which is much larger than that at the X line. The third term on the right-hand side of Eq. (2) is about $-\frac{2B_{xE}^2}{5\mu_0 L_E}\left(1-\frac{\delta_E^2}{L_E^2}\right)$.

Therefore, the electron outflow velocity just downstream of the EDR can be easily obtained from Eq. (2),

$$V_{exE} \approx V_{Ae}\left[\frac{1-S_L^2}{5\left(1+\frac{\delta_E^2}{d_e^{*2}}\right)}\right]^{1/2}, \tag{3}$$

where $V_{Ae}=\frac{B_{xE}}{\sqrt{\mu_0 m_e n_e}}$ is the electron Alfvén speed and d_e^* is the electron inertial length based on the plasma density n_e.

The x component of the ion momentum equation along the line $z=0$ can be described as follows:

$$n_i m_i\left(\frac{\partial V_{ix}}{\partial t}+V_{ix}\frac{\partial V_{ix}}{\partial x}\right)=j_{iy}B_z-en_iE_x-\frac{\partial P_{ixx}}{\partial x}. \tag{4}$$

The right-hand side of the equation illustrates the contributions from the Lorentz force, electric field, and pressure gradient term, and similarly, we can neglect the time derivative of the ion outflow velocity on the left-hand side. In the IDR (except the EDR), the electrons are magnetized, and then the electric field can be described as $\boldsymbol{E}=-\boldsymbol{V}_e\times\boldsymbol{B}$. Therefore, Eq. (4) can be written as,

$$n_i m_i V_{ix}\frac{\partial V_{ix}}{\partial x}=j_yB_z-\frac{\partial P_{ixx}}{\partial x}. \tag{5}$$

If the work done to the ions in the IDR is mainly converted to the ion enthalpy flux away from the IDR, then $p_{ixxI}\approx\frac{2B_{xI}^2}{5\mu_0}\left(1-\frac{\delta_I^2}{L_I^2}\right)$, which is much larger than that at the X line. In a similar way to that in the EDR, after assuming that the size of the IDR is much larger than that of the EDR, we can obtain the ion outflow velocity just downstream of the IDR,

$$V_{ixI}\approx\frac{V_{Ai}\left(1-S_L^2\right)}{\sqrt{5}}, \tag{6}$$

where $V_{Ai}=\frac{B_{xI}}{\sqrt{\mu_0 m_i n_i}}$ is the ion Alfvén speed based on the magnetic field B_{xI} and the plasma density n_i. Then,

$$\frac{V_{ixI}}{V_{exE}}\approx\frac{B_{xI}}{B_{xE}}\sqrt{\frac{m_e}{m_i}\left(1+\frac{\delta_E^2}{d_e^{*2}}\right)}. \tag{7}$$

When the reconnection rate approaches the peak value, the plasma is incompressible, and the plasma density is nearly uniform in the diffusion region, which is about the same as that of the background plasma of the Harris current sheet (n_b), that is $n_i\approx n_e\approx n_b$. At the same time, $V_{izI}L_I\approx V_{ixI}\delta_I$ and $V_{ezE}L_E\approx V_{exE}\delta_E$. The reconnection electric field is uniform in the inflow region, and $V_{izI}B_{xI}\approx V_{ezE}B_{xE}$. Based on these, we can obtain,

$$\frac{B_{xE}}{B_{xI}}\approx\frac{V_{ixI}}{V_{exE}}. \tag{8}$$

Combining Eqs. (7) and (8), we get,

$$\frac{B_{xE}}{B_{xI}}=\left[\frac{m_e}{m_i}\left(1+\frac{\delta_E^2}{d_e^{*2}}\right)\right]^{\frac{1}{4}}. \tag{9}$$

In the upstream of the IDR, the thermal pressure is assumed negligible, such that the inward-directed magnetic pressure gradient force is balanced by the outward-directed magnetic tension,[17] we have $\frac{B_{xI}}{B_0}\approx\frac{1-S_L^2}{1+S_L^2}$.

At last, the electron outflow speed on the downstream boundary of the EDR is

$$V_{exE}\approx\left(\frac{n_0}{5n_b}\right)^{1/2}V_{A0}\frac{1-S_L^2}{1+S_L^2}\left[\frac{m_i}{m_e}\left(\frac{(1-S_L^2)^2}{\left(1+\frac{\delta_E^2}{d_e^{*2}}\right)}\right)\right]^{1/4}. \tag{10}$$

Combining Eqs. (9) and (10), the reconnection electric field in the EDR ($E_{yE}=V_{exE}B_{zE}$) can be expressed as follows:

$$E_{yE}\approx\left(\frac{n_0}{5n_b}\right)^{1/2}S_L\left(\frac{1-S_L^2}{1+S_L^2}\right)^2\left(1-S_L^2\right)^{\frac{1}{2}}B_0V_{A0}. \tag{11}$$

At last, the reconnection rate when the reconnection electric field is normalized to B_0V_{A0} can be expressed as,

$$R\approx\left(\frac{n_0}{5n_b}\right)^{1/2}S_L\left(\frac{1-S_L^2}{1+S_L^2}\right)^2\left(1-S_L^2\right)^{\frac{1}{2}}. \tag{12}$$

In order to obtain Eq. (12), we have assumed that the plasma is incompressible, the aspect ratios of the EDR and IDR are the same, and the currents in the EDR and IDR are carried by the electrons and ions, respectively. These conditions are satisfied when magnetic reconnection has attained a well-developed state. Figure 2 shows the variation of $F=\frac{1}{\sqrt{5}}S_L\left(\frac{1-S_L^2}{1+S_L^2}\right)^2\sqrt{1-S_L^2}$ dependent on the aspect ratio S_L. F peaks at about 0.09 when the aspect ratio is $S_{Lp}\approx 0.34$. We assume that the reconnection rate rises with the increase in the aspect ratio and reaches the peak value about $R_{peak}=0.09\sqrt{n_0/n_b}$ at the aspect ratio $S_L=0.34$. The value is independent of the ion-to-electron mass ratio and is proportional to $\sqrt{n_0/n_b}$.

III. SIMULATION SETUP AND VALIDATION

Two-dimensional (2D) particle-in-cell (PIC) simulations have been conducted using the EPOCH PIC code to validate our theoretical model.[63] The initial equilibrium is a Harris current sheet in the

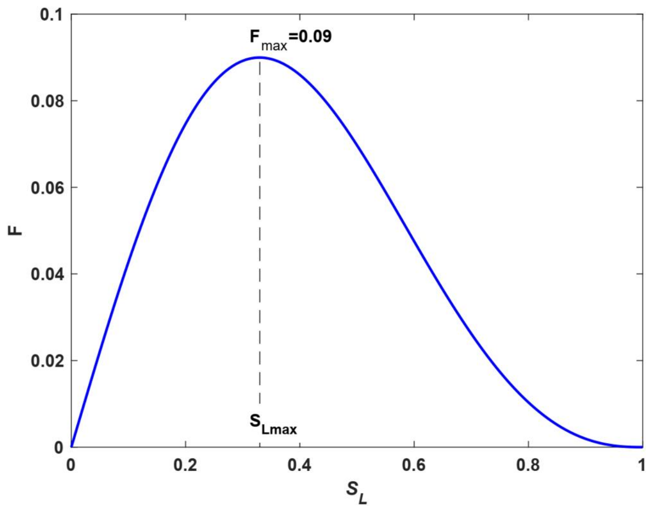

FIG. 2. The variation of $F = \frac{1}{\sqrt{5}} S_L \left(\frac{1-S_L^2}{1+S_L^2}\right)^2 \sqrt{1-S_L^2}$ dependent on the aspect ratio S_L. The value of F peaks ($F_{max} \approx 0.09$) when $S_{Lp} \approx 0.34$.

(x, z) plane, with a background density of $n_b = 0.08n_0$ (where n_0 is the peak density of the current sheet). Both ions and electrons initially follow the Maxwellian distribution, with the temperature ratio of $T_{i0}/T_{e0} = 4$ (where T_{e0} and T_{i0} denote the initial temperatures of electrons and ions, respectively). The simulation parameters are set as follows: the half-width of the current sheet is $\delta = 0.5d_i$ (where $d_i = c/\omega_{pi}$ is the ion inertial length based on n_0), the ion-to-electron mass ratio is $m_i/m_e = 100$, and the speed of light is $c = 15V_{A0}$ (where $V_{A0} = B_0/\sqrt{\mu_0 m_i n_0}$ is the Alfvén speed, and B_0 is the asymptotic magnetic field). The simulation domain spans $L_x \times L_z = 80d_i \times 20d_i$, with a spatial resolution of $\Delta x = \Delta z = 0.05d_i$. The time step is $\Delta t = 0.001\Omega_i^{-1}$ (where $\Omega_i = eB_0/m_i$ is the ion gyrofrequency). Periodic boundary conditions are applied in the x-direction, while conducting boundaries are used in the z-direction. No initial perturbation is introduced in the simulation.

Figure 2 shows the temporal evolution of (a1)–(a5), the reconnection electric field E_y, and (b1)–(b5) the nonideal electric field in the electron-frame $(\boldsymbol{E} + \boldsymbol{V}_e \times \boldsymbol{B})_y$. As the magnetic reconnection evolves, the reconnection electric field is induced near the X line. The EDR can be easily distinguished around the X line under a nonzero nonideal electric field in the electron-frame, satisfying $(\boldsymbol{E} + \boldsymbol{V}_e \times \boldsymbol{B})_y > 0$. Magnetic field pileup takes place downstream of the EDR, which initiates the generation of a pair of DFs that propagate continuously downstream. Notably, the reconnection electric field near the DFs increases more rapidly and eventually exceeds that around the X line.

We present the evolution of (a1)–(a5) the electron outflow velocity V_{ex} and (b1)–(b5) the ion outflow velocity V_{ix} in Fig. 3. Figures 3(c1)–3(c5) display the profiles of the electron outflow velocity V_{ex}, the ion outflow velocity V_{ix}, and the nonideal electric field in the electron-frame $(\boldsymbol{E} + \boldsymbol{V}_e \times \boldsymbol{B})_y$ along the line $z = 0$, while Figs. 3(d1)–3(d5) exhibit the reconnection electric field E_y and the magnetic field B_z along the same line. The electrons are accelerated and acquire an outflow velocity V_{ex} within the inner EDR. The electron outflow velocity V_{ex} becomes larger and larger when the electrons leave the X line and reaches the peak value downstream of the inner EDR. Meanwhile, the ion outflow velocity V_{ix} rises gradually as ions depart from the X line. Ions and electrons become coupled around the DF, where the magnetic field B_z attains its peak value, and the DFs can thus be regarded as the downstream boundary of the IDR.[19,61] It can also be observed from Figs. 2(d1)–2(d5) that the reconnection electric field is nearly uniform within the EDR.

Figure 4(a) shows the evolution of the reconnection electric field at three key locations: the X line E_{yX}, the immediate downstream region of the EDR E_{yE}, and the DF region E_{yI}. The evolution processes can be clearly divided into two distinct phases. In the first phase (Stage I), the reconnection rate R, defined as the normalized reconnection electric field at the X line $E_{yX}/(V_{A0}B_0)$, experiences a self-reinforcing process.[19,64] It initiates a sharp increase starting at approximately $\Omega_i t = 40$ and attains its peak value 0.46 around $\Omega_i t = 47$. In the subsequent phase (Stage II), the reconnection rate R exhibits a gradual decline from about $\Omega_i t = 47$. The reconnection electric field immediate downstream of the EDR is given by $E_{yE} = V_{exE}B_{zE}$ (where V_{exE} and B_{zE} denote the electron outflow velocity V_{ex} and magnetic field B_z at this position, respectively). In the vicinity of the DF, both ion and electron species become magnetized, and the corresponding reconnection electric field is formulated as $E_{yI} = V_{ixI}B_{zI}$ (with V_{ixI} and B_{zI} representing the ion outflow velocity V_{ix} and magnetic field B_z near the DF). It should be noted that the electron outflow velocity V_{ex} is nearly identical to the ion outflow velocity V_{ix} around the DF, i.e., $V_{ixI} \approx V_{exI}$. The magnitude of E_{yE} is roughly equivalent to that of the reconnection electric field at the X line. A pronounced discrepancy between E_{yI} and E_{yX} emerges at about $\Omega_i t = 47$ and widens progressively thereafter.

Figures 4(b)–4(f) depict the temporal variation profiles of multiple key physical parameters associated with magnetic reconnection, as elaborated below: (b) the half-lengths of the EDR and IDR, denoted as L_E and L_I, respectively, (c) the magnetic fields immediately downstream of the EDR and IDR, marked as B_{zE} and B_{zI}, respectively, (d) the aspect ratios of the EDR and IDR, defined as $S_{LE} = \delta_E/L_E$ (with δ_E representing the half-width of the EDR) and $S_{LI} = \delta_I/L_I$ (with δ_I referring to the half-width of the IDR), (e) the electron outflow velocity right downstream of the EDR V_{exE}, and the ion outflow velocity immediately downstream of the IDR V_{ixI}, and (f) the average magnitudes of the ion number density (n_i), electron density (n_e), ion current density (j_{iy}), and electron current density (j_{ey}) within the EDR. As visualized in Fig. 3(b), the length of the IDR exhibits a slow growth trend throughout Stage I, followed by a rapid downstream expansion in Stage II. In contrast, the length of the EDR remains nearly constant during Stage I and only initiates a gradual increment in the subsequent Stage II. In the process of magnetic reconnection, magnetic flux is transported from the upstream region to the downstream region via the X line, which gives rise to the enhancement of the downstream magnetic fields B_{zE} and B_{zI}. Nevertheless, as illustrated in Fig. 3(c), the magnetic field B_{zE} immediately downstream of the EDR starts to decline in Stage II, attributed to the downstream expansion of the EDR, while the magnetic field B_{zI} immediately downstream of the IDR surges sharply in the same stage.

According to Fig. 3(d), the aspect ratios of both the EDR and IDR rise continuously in Stage I and then drop gradually in Stage II; moreover, the two aspect ratios are roughly equivalent in Stage I, which stems from the straightening effect of magnetic tension on the magnetic field lines. The electron outflow velocity from the EDR V_{exE}

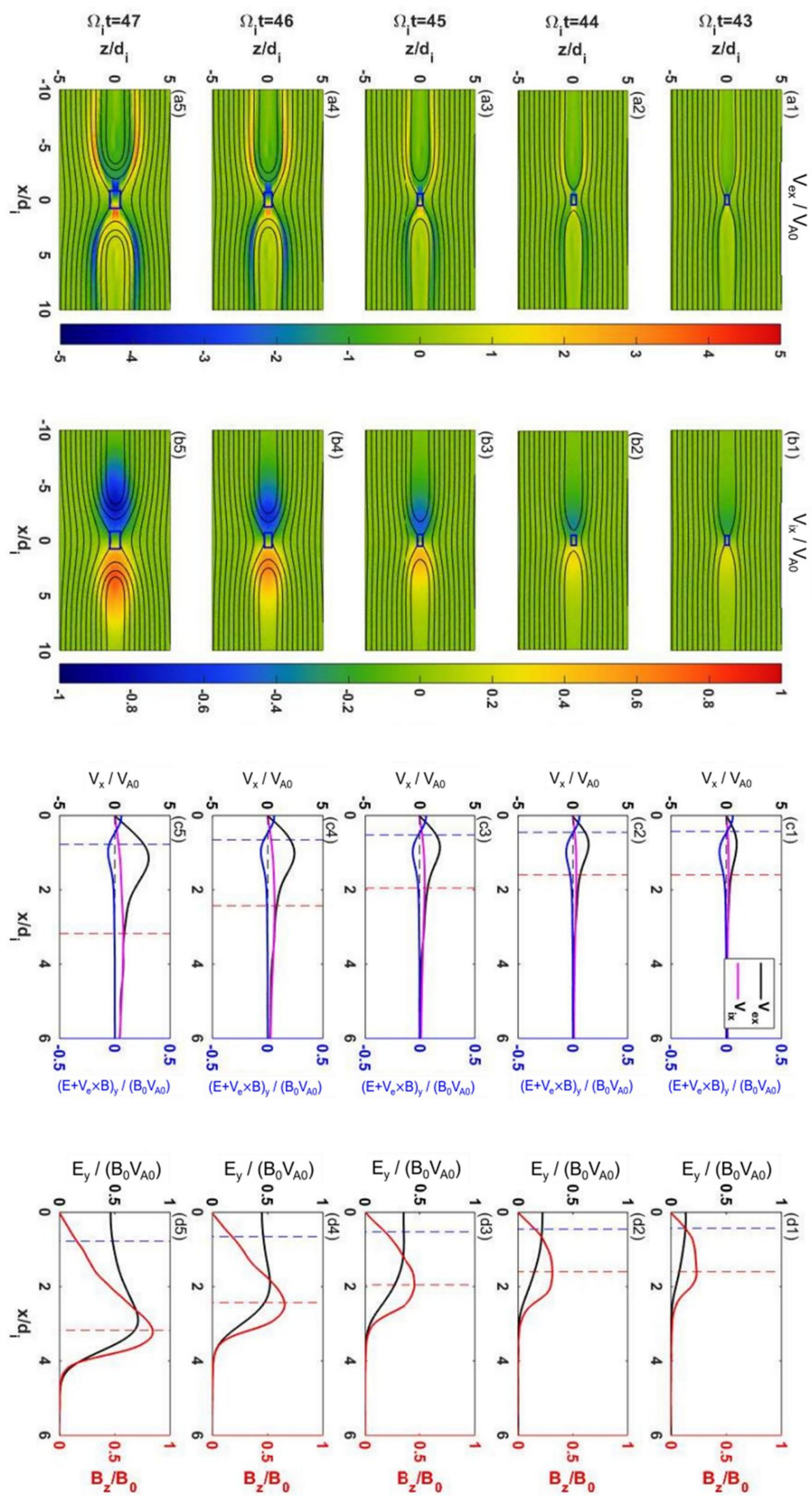

FIG. 3. The distribution of (a1)–(a5) the electron outflow velocity V_{ex} and (b1)–(b5) the ion outflow velocity V_{ix} at $\Omega_i t = 43$, 44, 45, 46, and 47. The profiles of (c1)–(c5) the electron outflow velocity V_{ex}, the ion outflow velocity V_{ix}, and the nonideal electric field $(\boldsymbol{E} + \boldsymbol{V}_e \times \boldsymbol{B})_y$, and (d1)–(d5) the reconnection electric field E_y and the magnetic field B_z along the line $z = 0$ at $\Omega_i t = 43$, 44, 45, 46, and 47.

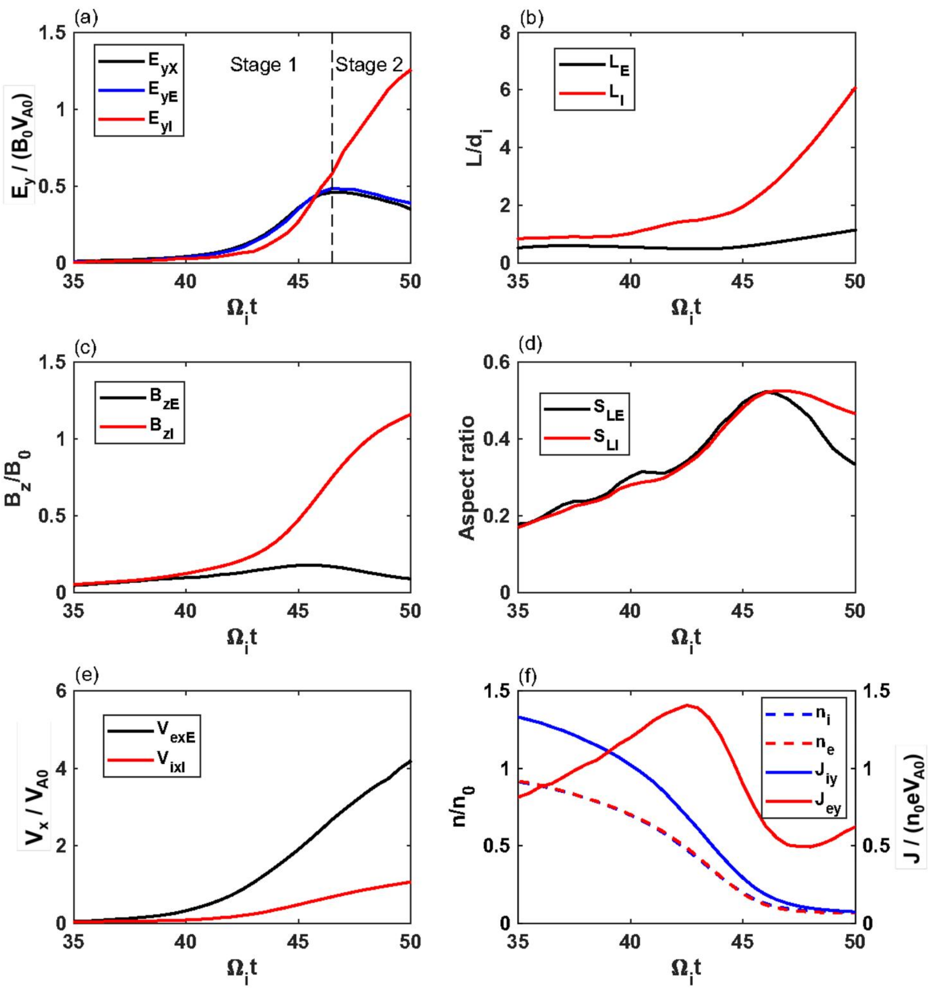

FIG. 4. The evolution of physical parameters around the X line. (a) The reconnection electric field at the X line (E_{yX}), at the just downstream of the EDR (E_{yE}), and at the just downstream of the IDR (E_{yI}). (b) The half-length of the EDR (L_E) and the half-length of the IDR (L_I). (c) The magnetic field just downstream of the EDR (B_{zE}) and that just downstream of the IDR(B_{zI}). (d) The aspect of the EDR $S_{LE} = \delta_E / L_E$ (where δ_E is the half-width of the EDR), and the aspect of the IDR $S_{LI} = \delta_I / L_I$ (where δ_I is the half-width of the IDR). (e) The electron outflow velocity just downstream of the EDR (V_{exE}) and the ion outflow velocity just downstream of the IDR V_{ixI}. (f) The average values of the ion number density (n_i), the electron density (n_e), the ion current density (j_{iy}), and electron current density (j_{ey}) in the EDR.

and the ion/electron outflow velocity from the IDR $V_{ixI} \approx V_{exI}$ both climb initially and reach a saturation state at approximately $\Omega_i t = 49$, with their peak values reaching around 4.2 and $1.0V_{A0}$, respectively, as presented in Fig. 3(e).

Figure 3(f) characterizes the evolutionary patterns of plasma densities and current densities within the EDR. The electron number density and ion number density in the inner EDR are nearly identical, and both decrease rapidly to roughly $0.08n_0$ during Stage I, which is

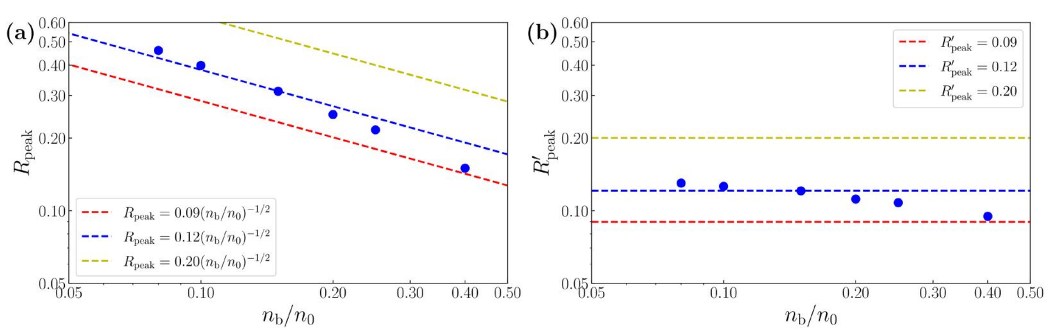

FIG. 5. The peak reconnection rates in different values of n_b/n_0, which is obtained in the simulations and the theoretical models. The simulation results are denoted by blue dots and fitted by the least squares method. The peak reconnection rates in different values of n_b/n_0 predicted by Lu *et al.*[19] and the theoretical model proposed in this paper are also plotted. (a) The peak reconnection rates obtained in the simulations can be approximated as $R_{peak} = 0.12\sqrt{n_0/n_b}$ when the reconnection electric field is normalized by $V_{A0}B_0$. (b) The peak reconnection rates obtained in the simulations can be approximated as $R'_{peak} = 0.12$ when the reconnection electric field is normalized by $V_{Ab}B_0$.

consistent with the background plasma density of the Harris current sheet. This variation trend further induces a synchronous evolution of the ion current density in the inner EDR. Since electrons inside the EDR are readily accelerated by the reconnection electric field, the electron current density increases initially and then decreases once electrons depart from the EDR. Notably, it can be observed that the electron current density far exceeds the ion current density after $\Omega_i t = 43$.

From the simulation results, we find that key assumptions in the theoretical model hold as the reconnection rate approaches its peak. These assumptions are as follows: (1) uniform reconnection electric field in the EDR; (2) the plasma density in the EDR drops down to the background plasma density; (3) uniform plasma density distribution across the diffusion region; (4) electron current dominates the current in the EDR; and (5) the aspect ratios of the EDR and IDR are approximately identical.

We also change the parameter n_0/n_b in the simulations while keeping the other parameters unchanged to verify the relation between the peak reconnection rate and $\sqrt{n_0/n_b}$ predicted by the theoretical model. Figure 5(a) compares the peak reconnection rates for different values of n_b/n_0, which is obtained in the simulations and the theoretical models. In the figure, the peak reconnection rates in different values of n_b/n_0 predicted by Lu *et al.*[19] are also plotted. The peak reconnection rates obtained in the simulations can be approximated as $R_{peak} = 0.12\sqrt{n_0/n_b}$.

If we normalize the reconnection electric field to $V_{Ab}B_0$ (where $V_{Ab} = B_0/\sqrt{\mu_0 m_i n_b}$ denotes the Alfvén speed evaluated using the background plasma density n_b), the peak reconnection rate derived from our theoretical model reads $R'_{peak} = 0.09$, a constant value close to 0.1. Figure 5(b) compares the peak reconnection rate normalized to $V_{Ab}B_0$ in different values of n_b/n_0, which is obtained in the simulations and theoretical models. The peak reconnection rates obtained in the simulations are around 0.12, although they slightly decrease with the increase in n_b/n_0. This may be caused by the thermal pressure, which cannot be negligible in the upstream of the IDR when n_b/n_0 is sufficiently large.

IV. CONCLUSIONS AND DISCUSSION

Recently, Lu *et al.*[19] proposed a first-principles theoretical model of the reconnection rate during non-steady collisionless reconnection in a Harris-type current sheet, where the ion and electron outflows are solely governed by the Lorentz force term, and the peak reconnection rate is approximated as $0.2\sqrt{n_0/n_b}$. In this paper, we extend the theoretical model developed in Lu *et al.*[19] by including the pressure gradient and electric field in the force-balance equation of ion and electron outflows. Compared with that in Lu *et al.*,[19] the peak reconnection rate predicted in our model is $0.2\sqrt{n_0/5n_b} \approx 0.09\sqrt{n_0/n_b}$. The parameter $1/\sqrt{5}$ comes from the pressure gradient. If we normalize the reconnection rate with $B_0 V_{Ab}$ (where $V_{Ab} = B_0/\sqrt{\mu_0 m_i n_b}$ is the Alfvén speed based on the background plasma density of the Harris-type current sheet), the peak reconnection rate should be 0.09. The value is nearly identical to the well-known reconnection rate (about 0.1) in collisionless magnetic reconnection, and in our simulations, the peak reconnection rate is estimated to be about 0.12. The difference may come from the assumption in the model, such as the incompressibility of the plasma in the diffusion region, and identical diagonal components for the electron and ion pressure tensors in the EDR and IDR.

It is also worth noting that our theoretical model for the reconnection rate neglects guide-field effects and is restricted to antiparallel reconnection with identical plasma parameters in both current-sheet lobes. Developing an extended theoretical model that quantifies the modulation of the reconnection rate by guide field and asymmetry of reconnection configuration constitutes a key direction for our future work.

ACKNOWLEDGMENTS

This work was supported by the National Key Research and Development Program of China (No. 2022YFA1604600) and the National Science Foundation of China (NSFC) (Grant No. 42304169).

AUTHOR DECLARATIONS

Conflict of Interest

The authors have no conflicts to disclose.

Author Contributions

Quanming Lu: Conceptualization (lead); Project administration (equal); Supervision (equal); Writing – original draft (lead); Writing – review & editing (equal). **Yukang Shu:** Methodology (lead); Visualization (lead). **San Lu:** Validation (equal); Writing – review & editing (equal). **Shiyong Huang:** Writing – review & editing (equal). **Shihang Hu:** Validation (equal). **Rongsheng Wang:** Validation (equal).

DATA AVAILABILITY

The data that support the findings of this study are openly available in Science Data Bank at https://doi.org/10.57760/sciencedb.space.03411, Ref. 65.

REFERENCES

[1] D. Biskamp, *Magnetic Reconnection in Plasmas* (Cambridge University Press, 2000).
[2] S. Wang and Q. Lu, *Collisionless Magnetic Reconnection* (Science Press, Beijing, 2019) (in Chinese).
[3] J. Lin and T. G. Forbes, "Effects of reconnection on the coronal mass ejection process," J. Geophys. Res.: Space Phys. **105**(A2), 2375–2392, https://doi.org/10.1029/1999JA900477 (2000).
[4] V. Angelopoulos, J. P. McFadden, D. Larson, C. W. Carlson, S. B. Mende, H. Frey, T. Phan, D. G. Sibeck, K.-H. Glassmeier, U. Auster, E. Donovan, I. R. Mann, I. J. Rae, C. T. Russell, A. Runov, X.-Z. Zhou, and L. Kepko, "Tail reconnection triggering substorm onset," Science **321**(5891), 931–935 (2008).
[5] M. Yamada, R. Kulsrud, and H. Ji, "Magnetic reconnection," Rev. Mod. Phys. **82**(1), 603–664 (2010).
[6] J. L. Burch, R. B. Torbert, T. D. Phan, L.-J. Chen, T. E. Moore, R. E. Ergun, J. P. Eastwood, D. J. Gershman, P. A. Cassak, M. R. Argall, S. Wang, M. Hesse, C. J. Pollock, B. L. Giles, R. Nakamura, B. H. Mauk, S. A. Fuselier, C. T. Russell, R. J. Strangeway, J. F. Drake, M. A. Shay, Y. V. Khotyaintsev, P.-A. Lindqvist, G. Marklund, F. D. Wilder, D. T. Young, K. Torkar, J. Goldstein, J. C. Dorelli, L. A. Avanov, M. Oka, D. N. Baker, A. N. Jaynes, K. A. Goodrich, I. J. Cohen, D. L. Turner, J. F. Fennell, J. B. Blake, J. Clemmons, M. Goldman, D. Newman, S. M. Petrinec, K. J. Trattner, B. Lavraud, P. H. Reiff, W. Baumjohann, W. Magnes, M. Steller, W. Lewis, Y. Saito, V. Coffey, and M.

Chandler, "Electron-scale measurements of magnetic reconnection in space," Science 352(6290), aaf2939 (2016).
[7]H. Ji, W. Daughton, J. Jara-Almonte, A. Le, A. Stanier, and J. Yoo, "Magnetic reconnection in the era of exascale computing and multiscale experiments," Nat. Rev. Phys. 4(4), 263–282 (2022).
[8]Q. Lu, H. Fu, R. Wang, and S. Lu, "Collisionless magnetic reconnection in the magnetosphere," Chin. Phys. B 31(8), 089401 (2022).
[9]R. Wang, S. Lu, S. Wang, X. Li, and Q. Lu, "Recent progress on magnetic reconnection by *in situ* measurements," Rev. Mod. Plasma Phys. 7(1), 27 (2023).
[10]K. Huang, W. Ling, H. Tang, J. Guan, J. Yang, J. Xie, G. Peng, H. Ma, N. Wang, T. Zhang, Z. Cao, S. Ren, Y. Ke, K. Han, Y. Dong, Y. Lu, E. Peng, and Q. Lu, "Laboratory realization of magnetopause-like reconnection in space plasma environment research facility (SPERF)," Geophys. Res. Lett. 52(20), e2025GL117351, https://doi.org/10.1029/2025GL117351 (2025).
[11]F. Yang, Q. Lu, Q. Zhang, J. Xie, X. Gao, Y. Ke, L. Tang, S. Hu, Y. Shu, Y. Liu, L. Sang, S. Lu, R. Wang, and W. Ding, "Laboratory observations of Hall magnetic field in electron-only magnetic reconnection with a guide field," Geophys. Res. Lett. 52(7), e2024GL114151, https://doi.org/10.1029/2024GL114151 (2025).
[12]E. N. Parker, "Sweet's mechanism for merging magnetic fields in conducting fluids," J. Geophys. Res. 62(4), 509–520, https://doi.org/10.1029/JZ062i004p00509 (1957).
[13]P. A. Sweet, "The neutral point theory of solar flares," Symp.-Int. Astron. Union 6, 123–134 (1958).
[14]H. E. Petschek, "Magnetic field annihilation," in *AAS/NASA Symposium on the Physics of Solar Flares*, edited by W. N. Ness (NASA, Washington, DC, 1964), p. 425.
[15]M. A. Shay and J. F. Drake, "The role of electron dissipation on the rate of collisionless magnetic reconnection," Geophys. Res. Lett. 25(20), 3759–3762, https://doi.org/10.1029/1998GL900036 (1998).
[16]P. A. Cassak, Y. H. Liu, and M. A. Shay, "A review of the 0.1 reconnection rate problem," J. Plasma Phys. 83(5), 715830501 (2017).
[17]Y. H. Liu, M. Hesse, F. Guo, W. Daughton, H. Li, P. A. Cassak, and M. A. Shay, "Why does steady-state magnetic reconnection have a maximum local rate of order 0.1?," Phys. Rev. Lett. 118(8), 085101 (2017).
[18]Y. H. Liu, P. Cassak, X. Li, M. Hesse, S. C. Lin, and K. Genestreti, "First-principles theory of the rate of magnetic reconnection in magnetospheric and solar plasmas," Commun. Phys. 5(1), 97 (2022).
[19]Q. Lu, Y. Shu, C. Chang, S. Lu, and R. Wang, "The rate of magnetic reconnection in non-steady state," Sci. Bull. 70(17), 2766–2770 (2025).
[20]E. N. Parker, "The solar-flare phenomenon and the theory of reconnection and annihiliation of magnetic fields," Astrophys. J., Suppl. Ser. 8, 177 (1963).
[21]Z. W. Ma and A. Bhattacharjee, "Hall magnetohydrodynamic reconnection: The geospace environment modeling challenge," J. Geophys. Res.: Space Phys. 106(A3), 3773–3782, https://doi.org/10.1029/1999JA001004 (2001).
[22]P. L. Pritchett, "Geospace environment modeling magnetic reconnection challenge: Simulations with a full particle electromagnetic code," J. Geophys. Res.: Space Phys. 106(A3), 3783–3798, https://doi.org/10.1029/1999JA001006 (2001).
[23]M. Øieroset, T. D. Phan, M. Fujimoto, R. P. Lin, and R. P. Lepping, "In situ detection of collisionless reconnection in the Earth's magnetotail," Nature 412(6845), 414–417 (2001).
[24]X. H. Deng and H. Matsumoto, "Rapid magnetic reconnection in the Earth's magnetosphere mediated by whistler waves," Nature 410(6828), 557–560 (2001).
[25]X. R. Fu, Q. M. Lu, and S. Wang, "The process of electron acceleration during collisionless magnetic reconnection," Phys. Plasmas 13(1), 012309 (2006).
[26]C. Huang, Q. Lu, and S. Wang, "The mechanisms of electron acceleration in antiparallel and guide field magnetic reconnection," Phys. Plasmas 17(7), 072306 (2010).
[27]M. Zhou, X. H. Deng, Z. H. Zhong, Y. Pang, R. X. Tang, M. El-Alaoui, R. J. Walker, C. T. Russell, G. Lapenta, R. J. Strangeway, R. B. Torbert, J. L. Burch, W. R. Paterson, B. L. Giles, Y. V. Khotyaintsev, R. E. Ergun, and P.-A. Lindqvist, "Observations of an electron diffusion region in symmetric reconnection with weak guide field," Astrophys. J. 870(1), 34 (2019).
[28]F. S. Mozer, S. D. Bale, J. P. McFadden, and R. B. Torbert, "New features of electron diffusion regions observed at subsolar magnetic field reconnection sites," Geophys. Res. Lett. 32(24), L24102, https://doi.org/10.1029/2005GL024092 (2005).
[29]Q. M. Lu, R. S. Wang, J. L. Xie, C. Huang, S. Lu, and S. Wang, "Electron dynamics in collisionless magnetic reconnection," Chin. Sci. Bull. 56(12), 1174–1181 (2011).
[30]A. Le, J. Egedal, O. Ohia, W. Daughton, H. Karimabadi, and V. S. Lukin, "Regimes of the electron diffusion region in magnetic reconnection," Phys. Rev. Lett. 110(13), 135004 (2013).
[31]M. Hesse, Y. Liu, L. Chen, N. Bessho, M. Kuznetsova, J. Birn, and J. L. Burch, "On the electron diffusion region in asymmetric reconnection with a guide magnetic field," Geophys. Res. Lett. 43(6), 2359–2364, https://doi.org/10.1002/2016GL068373 (2016).
[32]R. B. Torbert, J. L. Burch, T. D. Phan, M. Hesse, M. R. Argall, J. Shuster, R. E. Ergun, L. Alm, R. Nakamura, K. J. Genestreti, D. J. Gershman, W. R. Paterson, D. L. Turner, I. Cohen, B. L. Giles, C. J. Pollock, S. Wang, L. J. Chen, J. E. Stawarz, J. P. Eastwood, K. J. Hwang, C. Farrugia, I. Dors, H. Vaith, C. Mouikis, A. Ardakani, B. H. Mauk, S. A. Fuselier, C. T. Russell, R. J. Strangeway, T. E. Moore, J. F. Drake, M. A. Shay, Y. V. Khotyaintsev, P. A. Lindqvist, W. Baumjohann, F. D. Wilder, N. Ahmadi, J. C. Dorelli, L. A. Avanov, M. Oka, D. N. Baker, J. F. Fennell, J. B. Blake, A. N. Jaynes, O. Le Contel, S. M. Petrinec, B. Lavraud, and Y. Saito, "Electron-scale dynamics of the diffusion region during symmetric magnetic reconnection in space," Science 362(6421), 1391–1395 (2018).
[33]B. U. O. Sonnerup, "Magnetic field reconnection," in *Solar System Plasma Physics*, edited by L. J. Lanzerotti, C. F. Kennel, and E. N. Parker (North Holland Publishing Company, New York, 1979), p. 46.
[34]M. Hesse, K. Schindler, J. Birn, and M. Kuznetsova, "The diffusion region in collisionless magnetic reconnection," Phys. Plasmas 6(5), 1781–1795 (1999).
[35]F. S. Mozer, S. D. Bale, and T. D. Phan, "Evidence of diffusion regions at a subsolar magnetopause crossing," Phys. Rev. Lett. 89(1), 015002 (2002).
[36]A. Vaivads, Y. Khotyaintsev, M. André, A. Retinò, S. Buchert, B. Rogers, P. Décréau, G. Paschmann, and T. Phan, "Structure of the magnetic reconnection diffusion region from four-spacecraft observations," Phys. Rev. Lett. 93(10), 105001 (2004).
[37]Q. Lu, C. Huang, J. Xie, R. Wang, M. Wu, A. Vaivads, and S. Wang, "Features of separatrix regions in magnetic reconnection: Comparison of 2-D particle-in-cell simulations and cluster observations," J. Geophys. Res.: Space Phys. 115(11), A11208, https://doi.org/10.1029/2010JA015713 (2010).
[38]B. N. Rogers, R. E. Denton, and J. F. Drake, "Signatures of collisionless magnetic reconnection," J. Geophys. Res.: Space Phys. 108(A3), 1111 (2003).
[39]T. Nagai, I. Shinohara, M. Fujimoto, M. Hoshino, Y. Saito, S. Machida, and T. Mukai, "Geotail observations of the Hall current system: Evidence of magnetic reconnection in the magnetotail," J. Geophys. Res.: Space Phys. 106(A11), 25929–25949, https://doi.org/10.1029/2001JA900038 (2001).
[40]M. A. Shay, J. F. Drake, B. N. Rogers, and R. E. Denton, "The scaling of collisionless, magnetic reconnect ion for large systems," Geophys. Res. Lett. 26(14), 2163–2166, https://doi.org/10.1029/1999GL900481 (1999).
[41]J. Birn, J. F. Drake, M. A. Shay, B. N. Rogers, R. E. Denton, M. Hesse, M. Kuznetsova, Z. W. Ma, A. Bhattacharjee, A. Otto, and P. L. Pritchett, "Geospace environmental modeling (GEM) magnetic reconnection challenge," J. Geophys. Res.: Space Phys. 106(A3), 3715–3719, https://doi.org/10.1029/1999JA900449 (2001).
[42]T. D. Phan, B. U. Ö. Sonnerup, and R. P. Lin, "Fluid and kinetics signatures of reconnection at the dawn tail magnetopause: Wind observations," J. Geophys. Res.: Space Phys. 106(A11), 25489–25501, https://doi.org/10.1029/2001JA900054 (2001).
[43]C. J. Xiao, Z. Y. Pu, X. G. Wang, Z. W. Ma, S. Y. Fu, T. D. Phan, Q. G. Zong, Z. X. Liu, M. W. Dunlop, K.-H. Glassmeier, A. Balogh, H. Reme, I. Dandouras, and C. P. Escoubet, "A cluster measurement of fast magnetic reconnection in the magnetotail," Geophys. Res. Lett. 34(1), L01101, https://doi.org/10.1029/2006GL028006 (2007).
[44]Y.-H. Liu, W. Daughton, H. Karimabadi, H. Li, and S. Peter Gary, "Do dispersive waves play a role in collisionless magnetic reconnection?," Phys. Plasmas 21(2), 022113 (2014).

[45]E. N. Parker, "The reconnection rate of magnetic fields," Astrophys. J. **180**, 247 (1973).
[46]X. Li and Y.-H. Liu, "The effect of thermal pressure on collisionless magnetic reconnection rate," Astrophys. J. **912**(2), 152 (2021).
[47]H. W. Zhan, S. Y. Huang, Q. Y. Xiong, Z. G. Yuan, K. Jiang, Z. Wang, and Y. T. Tang, "An analytical model of reconnection rate in electron-only reconnection," Astrophys. J. **986**(2), 223 (2025).
[48]Y. Guan, Q. Lu, S. Lu, Y. Shu, and R. Wang, "Role of ion dynamics in electron-only magnetic reconnection," Geophys. Res. Lett. **51**(19), 2024GL110787, https://doi.org/10.1029/2024GL110787 (2024).
[49]Z. Wang, H. S. Fu, A. Vaivads, J. L. Burch, Y. Yu, and J. B. Cao, "Monitoring the spatio-temporal evolution of a reconnection x-line in space," Astrophys. J. Lett. **899**(2), L34 (2020).
[50]A. H. Tian, Z. Wang, H. S. Fu, and Z. Z. Guo, "Evidence of a magnetic null in electron-only reconnection," Geophys. Res. Lett. **52**(2), e2024GL113104, https://doi.org/10.1029/2024GL113104 (2025).
[51]A. Runov, V. Angelopoulos, M. I. Sitnov, V. A. Sergeev, J. Bonnell, J. P. McFadden, D. Larson, K. H. Glassmeier, and U. Auster, "THEMIS observations of an earthward-propagating dipolarization front," Geophys. Res. Lett. **36**(14), L14106, https://doi.org/10.1029/2009GL038980 (2009).
[52]M. I. Sitnov, M. Swisdak, and A. V. Divin, "Dipolarization fronts as a signature of transient reconnection in the magnetotail," J. Geophys. Res.: Space Phys. **114**(A4), A04202, https://doi.org/10.1029/2008JA013980 (2009).
[53]X. Deng, M. Ashour-Abdalla, M. Zhou, R. Walker, M. El-Alaoui, V. Angelopoulos, R. E. Ergun, and D. Schriver, "Wave and particle characteristics of earthward electron injections associated with dipolarization fronts," J. Geophys. Res.: Space Phys. **115**(9), A09225, https://doi.org/10.1029/2009JA015107 (2010).
[54]H. S. Fu, J. B. Cao, Y. V. Khotyaintsev, M. I. Sitnov, A. Runov, S. Y. Fu, M. Hamrin, M. André, A. Retinò, Y. D. Ma, H. Y. Lu, X. H. Wei, and S. Y. Huang, "Dipolarization fronts as a consequence of transient reconnection: In situ evidence," Geophys. Res. Lett. **40**(23), 6023–6027, https://doi.org/10.1002/2013GL058620 (2013).
[55]S. Lu, Q. Lu, Y. Lin, X. Wang, Y. Ge, R. Wang, M. Zhou, H. Fu, C. Huang, M. Wu, and S. Wang, "Dipolarization fronts as earthward propagating flux ropes: A three-dimensional global hybrid simulation," J. Geophys. Res.: Space Phys. **120**(8), 6286–6300, https://doi.org/10.1002/2015JA021213 (2015).
[56]S. Y. Huang, H. S. Fu, Z. G. Yuan, M. Zhou, S. Fu, X. H. Deng, W. J. Sun, Y. Pang, D. D. Wang, H. M. Li, H. M. Li, and X. D. Yu, "Electromagnetic energy conversion at dipolarization fronts: Multispacecraft results," J. Geophys. Res.: Space Phys. **120**(6), 4496–4502, https://doi.org/10.1002/2015JA021083 (2015).
[57]Y. Shu, S. Lu, Q. Lu, W. Ding, and S. Wang, "Energy budgets from collisionless magnetic reconnection site to reconnection front," J. Geophys. Res.: Space Phys. **126**(10), e2021JA029712, https://doi.org/10.1029/2021JA029712 (2021).
[58]C. Chang, Q. Lu, S. Lu, K. Huang, and R. Wang, "Ion and electron motions in the outer electron diffusion region of collisionless magnetic reconnection," Earth Planet. Phys. **8**(3), 472–478 (2024).
[59]C. Huang, Q. Lu, F. Guo, M. Wu, A. Du, and S. Wang, "Magnetic islands formed due to the Kelvin–Helmholtz instability in the outflow region of collisionless magnetic reconnection," Geophys. Res. Lett. **42**(18), 7282–7286, https://doi.org/10.1002/2015GL065690 (2015).
[60]J. Egedal, W. Daughton, A. Le, and A. L. Borg, "Double layer electric fields aiding the production of energetic flat-top distributions and superthermal electrons within magnetic reconnection exhausts," Phys. Plasmas **22**(10), 101208 (2015).
[61]S. Hu, Q. Lu, Y. Shu, S. Lu, K. Huang, and J. Nan, "Electrostatic field formed by charge separation in antiparallel magnetic reconnection," Astrophys. J. **986**(1), 43 (2025).
[62]H. S. Fu, Z. Wang, and J. B. Cao, "Fundamental understanding of magnetic reconnection via spiral CT scan. III. Electron agyrotropy and temperature anisotropy," Astrophys. J. **985**(2), 168 (2025).
[63]T. D. Arber, K. Bennett, C. S. Brady, A. Lawrence-Douglas, M. G. Ramsay, N. J. Sircombe, P. Gillies, R. G. Evans, H. Schmitz, A. R. Bell, and C. P. Ridgers, "Contemporary particle-in-cell approach to laser-plasma modelling," Plasma Phys. Controlled Fusion **57**(11), 113001 (2015).
[64]Q. Lu, S. Lu, C. Huang, M. Wu, and S. Wang, "Self-reinforcing process of the reconnection electric field in the electron diffusion region and onset of collisionless magnetic reconnection," Plasma Phys. Controlled Fusion **55**(8), 085019 (2013).
[65]Q. Lu and Y. Shu (2026). "A first-principles theoretical model of the reconnection rate in non-steady magnetic reconnection," Science Data Bank, V. 1. https://doi.org/10.57760/sciencedb.space.03411